Quasistable two-dimensional solitons with hidden and explicit vorticity in a medium with competing nonlinearities

Hervé Leblond,[1] Boris A. Malomed,[2] and Dumitru Mihalache[3]
[1]*Laboratoire POMA, UMR 6136, Université d'Angers, 2 Bd Lavoisier, 49000 Angers, France*
[2]*Department of Interdisciplinary Studies, School of Electrical Engineering, Faculty of Engineering, Tel Aviv University, Tel Aviv 69978, Israel*
[3]*Department of Theoretical Physics, Institute of Atomic Physics, P.O. Box MG-6, Bucharest, Romania*
(Received 25 August 2004; published 15 March 2005)

We consider basic types of two-dimensional (2D) vortex solitons in a three-wave model combining quadratic $\chi^{(2)}$ and self-defocusing cubic $\chi_{-}^{(3)}$ nonlinearities. The system involves two fundamental-frequency (FF) waves with orthogonal polarizations and a single second-harmonic (SH) one. The model makes it possible to introduce a 2D soliton, with *hidden vorticity* (HV). Its vorticities in the two FF components are $S_{1,2}=\pm 1$, whereas the SH carries no vorticity, $S_3=0$. We also consider an ordinary compound vortex, with $2S_1=2S_2=S_3=2$. Without the $\chi_{-}^{(3)}$ terms, the HV soliton and the ordinary vortex are moderately unstable. Within the propagation distance $z\simeq 15$ diffraction lengths, Z_{diffr}, the former one turns itself into a usual zero-vorticity (ZV) soliton, while the latter splits into three ZV solitons (the splinters form a necklace pattern, with its own intrinsic dynamics). To gain analytical insight into the azimuthal instability of the HV solitons, we also consider its one-dimensional counterpart, viz., the modulational instability (MI) of a one-dimensional CW (continuous-wave) state with "hidden momentum," i.e., *opposite wave numbers* in its two components, concluding that such wave numbers may partly suppress the MI. As concerns analytical results, we also find exact solutions for spreading localized vortices in the 2D linear model; in terms of quantum mechanics, these are coherent states with angular momentum (we need these solutions to accurately define the diffraction length of the true solitons). The addition of the $\chi_{-}^{(3)}$ interaction strongly stabilizes both the HV solitons and the ordinary vortices, helping them to persist over z up to 50 Z_{diffr}. In terms of the possible experiment, they are completely stable objects. After very long propagation, the HV soliton splits into two ZV solitons, while the vortex with $S_3=2S_{1,2}=2$ splits into a set of three or four ZV solitons.

DOI: 10.1103/PhysRevE.71.036608 PACS number(s): 42.65.Tg

I. INTRODUCTION

Two-dimensional (2D) spatial solitons with embedded vorticity S constitute a class of topologically charged localized nonlinear modes in optical media, which have recently drawn a lot of interest, starting with the work that predicted (by means of direct simulations) stable vortices with $S=1$ in a model based on the 2D nonlinear Schrödinger equation with competing self-focusing cubic and self-defocusing quintic nonlinearities [1]. Further analysis had supported this result by showing that the spectrum of eigenmodes of small perturbations around the vortex solitons does not contain unstable eigenvalues, provided that the soliton's integral power (quadratic norm) exceeds a certain minimum value (in other words, the external size of the corresponding annulus-shaped soliton must be large enough), see details in Ref. [2]. It had also been found that higher-order vortex solitons in the 2D cubic-quintic (CQ) model have their stability regions for $S=2$ [2] (a short review of the topic was given in Ref. [3]), and also for $S>2$ (at least, up to $S=5$), although for $S\geqslant 3$ the stability region is very narrow, corresponding to the vortex solitons with an extremely large size [4,5].

A problem hampering experimental observation of the stable vortex solitons is that optical media, which may be approximated by the CQ nonlinear Schrödinger (NLS) equation (these are chalcogenide glasses [6] and some organic substances [7]), feature quite strong nonlinear loss (two-photon absorption) alongside the CQ nonlinearity [8], which can easily kill any soliton [9]. For this reason, and also because it was necessary to understand how general the conclusion about the existence of stable spatial vortex solitons was, this issue was further investigated in another model, which is also based on competing nonlinearities, viz., quadratic $\chi^{(2)}$ (alias second-harmonic-generating) and *self-defocusing* cubic $\chi_{-}^{(3)}$ terms (without the latter one, all the vortex solitons in $\chi^{(2)}$ media are subject to strong instability against azimuthal perturbations, which splits them into a set of separating zero-vorticity (ZV) stable solitons, as was shown both theoretically [10] and experimentally [11]). For the first time, *stable* vortices with $S=1$ and $S=2$ (which were called vortex rings, because of their annular shape) in the combined $\chi^{(2)}:\chi_{-}^{(3)}$ model were found in Ref. [12]. The stability was demonstrated through the calculation of stability eigenvalues and verified by direct simulations (see a brief review in Ref. [13]). Recently, this analysis was extended to higher-order solitons, with a conclusion that, as well as in the CQ model, the vortex rings with $S>2$ have their narrow stability regions, corresponding to the rings with a very large outer radius [14].

The $\chi^{(2)}$ models involve, at least, two waves—the fundamental-frequency (FF) and second-harmonic (SH) ones. The soliton's vorticity S is carried by the FF wave, whereas the SH vorticity is $2S$. In the real experiment, the FF-SH phase matching, which is a necessary condition for

the creation of solitons, can be more easily achieved using the natural birefringence of the $\chi^{(2)}$ crystal through the so-called type-II quadratic interaction. The latter involves two FF waves with orthogonal polarizations and a single SH wave [15,16]. In this case, the vorticities $S_{1,2}$ and S_3 of the two FF and one SH components are related in an obvious way, $S_1+S_2=S_3$. In particular, the configuration with $S_1=S_2=1$ and $S_3=2$ is a straightforward generalization of the fundamental vortex ring, with the vorticities 1 and 2 in the FF and SH waves, in the type-I $\chi^{(2)}$ model, which involves the single FF component [12]. However, a different species of the 2D soliton is the one with $S_1=-S_2=1$ and $S_3=0$, which is possible solely in the type-II system. For obvious reasons, this may be called a *hidden-vorticity* (HV) soliton.

It is relevant to mention that compound vortex solitons were recently studied in multicomponent models, such as a bimodal CQ system [17]. Another example is provided by a two-component system with saturable nonlinearity, with the vorticities $S_1=1$, $S_2=0$ [18]. The type-II system with the mixed $\chi^{(2)}:\chi_{-}^{(3)}$ nonlinearity is a very natural model to introduce spatial 2D solitons of the HV type, which were not considered in the above-mentioned models.

Although various types of solitons supported by the competing $\chi^{(2)}$ and $\chi^{(3)}$ nonlinearities in the type-I model have been studied in detail (see reviews [16]), their study in the three-wave type-II system was only recently started in Ref. [19], which dealt with one-dimensional (1D) solitons in this system. It has been found that, in some cases, the 1D solitons are drastically different, as concerns their stability, from their counterparts in both the two-wave $\chi^{(2)}:\chi^{(3)}$ model of type I and in the well-known two-wave model with the Kerr nonlinearity and birefringence, but without the $\chi^{(2)}$ interaction [20]. We also note that, while it may be difficult to find natural optical materials featuring the combined $\chi^{(2)}:\chi_{-}^{(3)}$ nonlinearity, it can be engineered, on the basis of materials with the usual $\chi^{(2)}$ nonlinearity, in various ways by means of the quasi-phase-matching technique [21,22] (see a detailed discussion in Ref. [19]).

Following Refs. [12,19], we adopt the following model governing the spatial evolution of two FF waves with the orthogonal polarizations and the single SH wave, coupled to them by the quadratic and cubic nonlinearities. In a normalized form, the equations for the corresponding local amplitudes $A_{1,2}$ and A_3 are

$$\left(i\frac{\partial}{\partial z}+\frac{1}{2}\nabla_{\perp}^2-\beta\right)A_1+A_2^*A_3-\frac{\lambda}{4}\left(|A_1|^2+\frac{2}{3}|A_2|^2\right)A_1-2\lambda|A_3|^2A_1=0, \tag{1}$$

$$\left(i\frac{\partial}{\partial z}+\frac{1}{2}\nabla_{\perp}^2-\frac{1}{\beta}\right)A_2+A_1^*A_3-\frac{\lambda}{4}\left(|A_2|^2+\frac{2}{3}|A_1|^2\right)A_2-2\lambda|A_3|^2A_2=0, \tag{2}$$

$$\left(2i\frac{\partial}{\partial z}+\frac{1}{2}\nabla_{\perp}^2-2\alpha\right)A_3+A_1A_2-\lambda(4|A_3|^2+2|A_1|^2+2|A_2|^2)A_3=0, \tag{3}$$

where z is the propagation distance, the Laplacian (diffraction operator) acts on the transverse coordinates (x,y), $\lambda>0$ is the relative strength of the $\chi_{-}^{(3)}$ nonlinearity (while the strength of the $\chi^{(2)}$ interaction is normalized to be 1), and real parameters β and α account, respectively, for the birefringence between the two FF polarizations and the residual phase-velocity mismatch between the FF and SH waves.

Equations (1)–(3) do not include the $\chi^{(3)}$-induced four-wave mixing (FWM) terms, such as $-(\lambda/12)A_2^2A_1^*$ and $-(\lambda/6)|A_2|^2A_3$, which were included in the full model put forward in Ref. [19]. Indeed, the phase-matching conditions for the FWM differ from those for the type-II coupling. Therefore, in the real experiments running close to the phase-matching point for the type-II interaction, the FWM is not expected to be phase matched. This argument allows us to neglect the corresponding terms in Eqs. (1)–(3).

As well as a majority of works in this field, the model disregards a possible dc field produced by rectification in the $\chi^{(2)}$ medium. Although the rectification may be a significant factor under special circumstances [23,24], it is unlikely that the special polarization conditions, which are required for the generation of the dc field [24], would be met simultaneously with those that are necessary for the efficient type-II $\chi^{(2)}$ interaction.

In this paper, we focus on the most fundamental type of HV solitons, i.e., the one with $S_{1,2}=\pm1$ and $S_3=0$, as said above. Note that the total angular momentum of the HV solitons is zero only in the case of $\beta=1$ in Eqs. (1) and (2), when the birefringence between the FF waves is absent; otherwise, the asymmetry between the A_1 and A_2 fields will give rise to a nonzero sum of their intrinsic angular momenta. We will also study, in parallel, ordinary vortex solitons in the same system, with $S_{1,2}=1$ and $S_3=2$.

First, we will briefly consider the proper $\chi^{(2)}$ version of the model, setting $\lambda=0$ in Eqs. (1)–(3). As might be expected, all the vortex solitons are unstable in this case, although the instability of both the HV and ordinary vortex solitons is moderate, requiring $\simeq 15$ diffraction lengths for its complete development. The HV soliton eventually transforms into an ordinary stable ZV (ground-state) soliton, while the ordinary vortex splits into a necklace pattern composed of three ZV solitons.

As is known, it is difficult to explain peculiarities of the azimuthal instability of vortex solitons in an analytical form (sometimes, it may be understood as an instability of the central hole in a large-area soliton against spontaneous off-center shift caused by its attraction to the outer rim of the soliton [2], but this instability mode is seldom a dominant one). To get, at least, some insight into the instability of the HV solitons, we will consider its 1D counterpart in the form of the modulational instability (MI) of a CW (continuous-wave) solution with *opposite wave numbers* of two FF components. Even this case turns out to be quite cumbersome in the general case; therefore, our actual analysis focuses on the cascading limit (corresponding to a large mismatch between the FF and SH fields [16]), wherein the type-II $\chi^{(2)}$ model goes over into a system of two cross-phase modulation (XPM)-coupled NLS equations. We demonstrate that the hidden momentum may attenuate the MI, which suggests an explanation for the relative stability of the HV solitons.

An issue of principle interest is a possibility to stabilize the vortices by means of the $\chi_{-}^{(3)}$ nonlinearity. Our main result is that, while complete stabilization of the HV soliton is not plausible (although we were not able to explore the entire parameter space of the model), the $\chi_{-}^{(3)}$ terms significantly attenuate the azimuthal instability, allowing the soliton to support itself over the propagation distance z equivalent to tens of diffraction lengths. This result puts the HV solitons in the $\chi^{(2)}:\chi_{-}^{(3)}$ model in the general class of *nearly stable* solitons, which, strictly speaking, do not exist or are unstable, but may be observed in the experiment, as their instability develops at unrealistically large values of z, which would definitely exceed the size of available samples. Examples of such objects are temporal [25] and spatiotemporal [26] solitons in $\chi^{(2)}$ media with normal group-velocity dispersion at the SH, which, generally, ought not to exist, but are, in effect, relevant physical objects (although not yet created in the experiment) because their decay would be extremely slow.

In order to bring the consideration closer to the experimental situation, we do not search for stationary solitons whose stability would be then tested by simulations. Instead, we start with an initial configuration that is expected to be sufficiently close to a stationary soliton. This corresponds to the way the experiment is run, starting with an initial beam that is believed to be sufficiently close to the soliton's profile. Because the initial configuration is not an exact solution, the spatial solitons observed in the direct simulations (both HV solitons and ordinary vortices), remaining *stable* against azimuthal perturbations, perform several cycles of slow oscillations in the radial direction (if the azimuthal perturbations are not seeded, then the number of the radial oscillations is indefinitely large, without invoking any instability).

To conclude the description of the topic, we note that 2D spatial solitons can be naturally generalized in the form of three-dimensional (3D) *spatiotemporal* solitons (STS), which brings the temporal variable into the model. In the $\chi^{(2)}:\chi_{-}^{(3)}$ model of type I, stable spinning STS, with the vorticities $S_1=1$ and $S_2=2$ in their FF and SH components, were predicted in Ref. [27]. Search for three-dimensional STS with hidden vorticity in the $\chi^{(2)}:\chi_{-}^{(3)}$ model of type II is a challenging issue, which is, however, very difficult in its technical aspects and will not be considered in the present paper.

The paper is organized as follows. In Sec. II we give an accurate definition of the above-mentioned diffraction length Z_{diffr}, using an exact vorticity-carrying solution to the linear 2D Schrödinger equation, which is based on a radial Gaussian. The accurate definition of Z_{diffr} is necessary, as the stable-propagation distance in the nonlinear models should be expressed in units of Z_{diffr}. Then, in Sec. III we present results concerning the azimuthal instability of the vortices in the $\chi^{(2)}$ model, with $\lambda=0$ in Eqs. (1)–(3). This is followed by brief consideration of the related issue of the modulational instability of the 1D CW states with the "hidden momentum" in Sec. IV. The main findings, demonstrating the instability inhibition by the $\chi_{-}^{(3)}$ terms, are reported in Sec. V. The paper is concluded by Sec. VI.

II. DIFFRACTION LENGTH FOR THE LINEAR VORTEX

In the linear approximation, Eqs. (1)–(3) decouple. Therefore, to define Z_{diffr}, which is determined by the linear parts of the equations, we take, e.g., the linear version of Eq. (1). A family of exact solutions can be found for it,

$$A_1(r,\theta,z)=A^{(0)}\frac{r^{S_1}}{(1+iz/r_0^2)^{(1+S_1)}}\exp\left(-i\beta z+iS_1\theta-\frac{1-iz/r_0^2}{1+z^2/r_0^4}\frac{r^2}{2r_0^2}\right), \tag{4}$$

where r and θ are the polar coordinates in the transverse plane, the integer $S_1\geqslant 0$ is the vorticity in the field A_1, while $A^{(0)}$ and r_0 are arbitrary constants. In terms of quantum mechanics, this solution can be understood as a 2D *coherent state* with the angular momentum S_1 in the two-dimensional free space.

The intensity distribution corresponding to the solution (4) is

$$|A_1(r,z)|^2=|A^{(0)}|^2\frac{r^{2S_1}}{(1+z^2/r_0^4)^{(1+S_1)}}\exp\left(-\frac{r^2}{r_0^2+z^2/r_0^2}\right). \tag{5}$$

It attains a maximum value at $r=\rho$, with

$$\rho=\sqrt{S_1(r_0^2+z^2/r_0^2)}, \tag{6}$$

which may be naturally identified as the radial size of the expanding vortex ring. Then, $\rho_0\equiv\sqrt{S_1}r_0$ is the initial size of the ring at the input point $z=0$, and Z_{diffr} may be defined as the propagation distance after which the ring's size becomes twice as large as it was at the input, $\rho(z=Z_{\mathrm{diffr}})=2\rho_0$. From this definition and Eq. (6), we find

$$Z_{\mathrm{diffr}}=(\sqrt{3}/S_1)\rho_0^2. \tag{7}$$

This expression will be used to gauge various propagation distances that emerge in simulations of the full nonlinear system.

An alternative definition of the vortex-ring's radius may be based, instead of the intensity profile (5), on the radial distribution of the intensity integrated over the angular variable θ, which implies the multiplication of Eq. (5) by $2\pi r$. The accordingly modified radius of the vortex ring and diffraction length amount to the same expressions (6) and (7) with S_1 replaced by $S_1+1/2$. Note that the expression (7) does not apply to the ZV pulse, with $S_1=0$. However, the alternative definition is also meaningful in this case, yielding $Z_{\mathrm{diffr}}^{(S=0)}=2\sqrt{3}\rho_0^2\equiv\sqrt{3}r_0^2$.

III. AZIMUTHAL INSTABILITY OF VORTICES IN THE $\chi^{(2)}$ MODEL

Numerical solution of the underlying equations (1)–(3) was performed by means of the Fourier decomposition in the angular variable θ,

$$A_j(r,\theta,z)=\sum_{p=-\infty}^{+\infty}A_j^{(p)}(r,z)e^{ip\theta},\quad j=1,2,3. \tag{8}$$

The substitution of Eq. (8) into Eqs. (1)–(3) leads to a chain of coupled equations with the independent variables r and z.

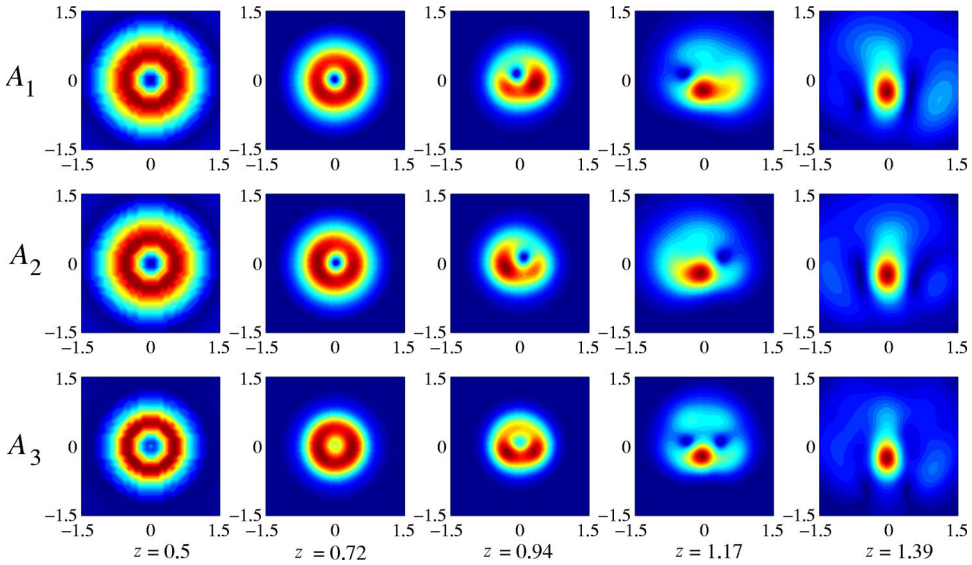

FIG. 1. (Color online) The contour plots show a typical example of the instability development for the soliton with the hidden vorticity, i.e., with the initial vorticities $(S_{1,2}=\pm 1, S_3=0)$, in the case of the positive mismatch, $\alpha=4$. In this example, the birefringence between the two components of the fundamental-frequency wave is absent, i.e., $\beta=1$.

This chain was truncated by dropping the amplitudes $A_j^{(p)}$ with $|p|>6$ (i.e., 13 azimuthal modes were taken into account). The evolution equations for the amplitudes $A_j^{(p)}$ were solved by means of a finite-differences scheme for r and z, with the usual three-point approximation for $\partial^2 A_j^{(p)}/\partial r^2$, and the three-point approximation for $\partial A_j^{(p)}/\partial z$, which provided for numerical stability of the scheme. We used a constant step $\delta z \simeq 5\times 10^{-6}$ for z, and the grid contained 100 points in the r direction, separated by a step $\delta r \simeq 0.08$. Actually, 35 of these points were involved in implementation of reflectionless absorbing boundary conditions at $r\to\infty$, which was done by adding linear-absorption terms to the equations over the set of 35 sites.

Furthermore, care was also taken to properly regularize the numerical scheme at $r\to 0$. This allowed us to avoid instability due to the factor r^{-1} in the radial part of the Laplacian.

Note that Eqs. (1)–(3) admit the substitution (8) with only three nonzero amplitudes $A_j^{(p_j)}$, provided that their azimuthal indices are locked so that $p_1+p_2=p_3$. In this case, the resulting equations for the three amplitudes easily generate a large number of solitary pulsons, i.e., solutions that are localized in r and feature periodic shape oscillations. These solutions are stable within the framework of the three-amplitude reduction. However, in the case of $\lambda=0$, which corresponds to the purely quadratic nonlinearity, small azimuthal perturbations, which include angular harmonics different from the initial triplet, easily trigger an instability. The azimuthal instability of the pulsons was also verified in the linear approximation by numerically computing eigenvalues that determine the instability growth rate for small perturbations.

As said above, we are, first of all, interested in the HV soliton, which is based on the expression (8) with the nonzero amplitudes $A_1^{(+1)}$, $A_2^{(-1)}$, and $A_3^{(0)}$. In this case, the fastest-growing azimuthal instability involves the angular harmonics of the perturbation with $p_{1,2}=0$ in the FF fields, and $p_3=\pm 1$ in the SH field. After the onset of the instability, higher-order angular harmonics are also generated.

The development of the azimuthal instability of the HV soliton eventually transforms it into an ordinary ZV soliton, which contains the single amplitude with $p=0$ in each field component. It is well known that the ZV soliton may easily be stable in $\chi^{(2)}$ models [16]. The actual mode of the instability-induced transformation of the HV soliton into the ZV soliton essentially depends on the sign of the mismatch parameter α [see Eq. (3)]. In the case of $\alpha>0$, Fig. 1 demonstrates that the soliton keeps its annular structure for a while (the SH component, which had no inner "hole" initially, also acquires a ring-shaped form). The ring gradually develops inhomogeneity in the azimuthal direction and, eventually, collects all the power into a single spot shifted relative to the center of the initial ring. Thus, the center of the eventually established ZV soliton is displaced relative to the center of the original HV soliton. In the opposite case, $\alpha<0$, the annular structure disappears faster, as is shown in Fig. 2.

Note that the initial data at $z=0$ in Figs. 1 and 2 have been chosen close to the final stage of the instability development, in order to focus on the crucial phase of the destruction of the vortices. This explains the strongly perturbed initial profile of the vortex ring in these figures. Longer simulations demonstrate that, if the perturbations at $z=0$ are much weaker (close to the precision of the numerical scheme), the destruction of the ring occurs at about $z=2.8$. Note that the ring's radius, identified as the position of the intensity maximum, is $\rho_0 \simeq 0.32$; hence, Eq. (7) yields $Z_{\mathrm{diffr}} \simeq 0.18$ (i.e., the destruction of the ring initiated by small perturbations occurs within 15 or 16 diffraction lengths), and the formation of the eventual ZV spot takes an additional one or two Z_{diffr}. In that case, the ring, being a pulson (see above), performs about one radial pulsation before it gets destroyed.

In the same model with $\lambda=0$, the ordinary vortex soliton, with the vorticities $S_{1,2}=1$ and $S_3=3$, is subject to the usual azimuthal instability, which splits it into a set of three stable ground-state (ZV) solitons. This outcome is illustrated by Fig. 3. In this case, too, the splitting proceeds very quickly because of the strong perturbation included in the initial configuration. If, instead, the same simulation is run with a small initial perturbation (with the relative amplitude $\sim 10^{-8}$), then the corresponding pulson performs about two oscillations in the radial direction, within a distance $z\simeq 1$, before the insta-

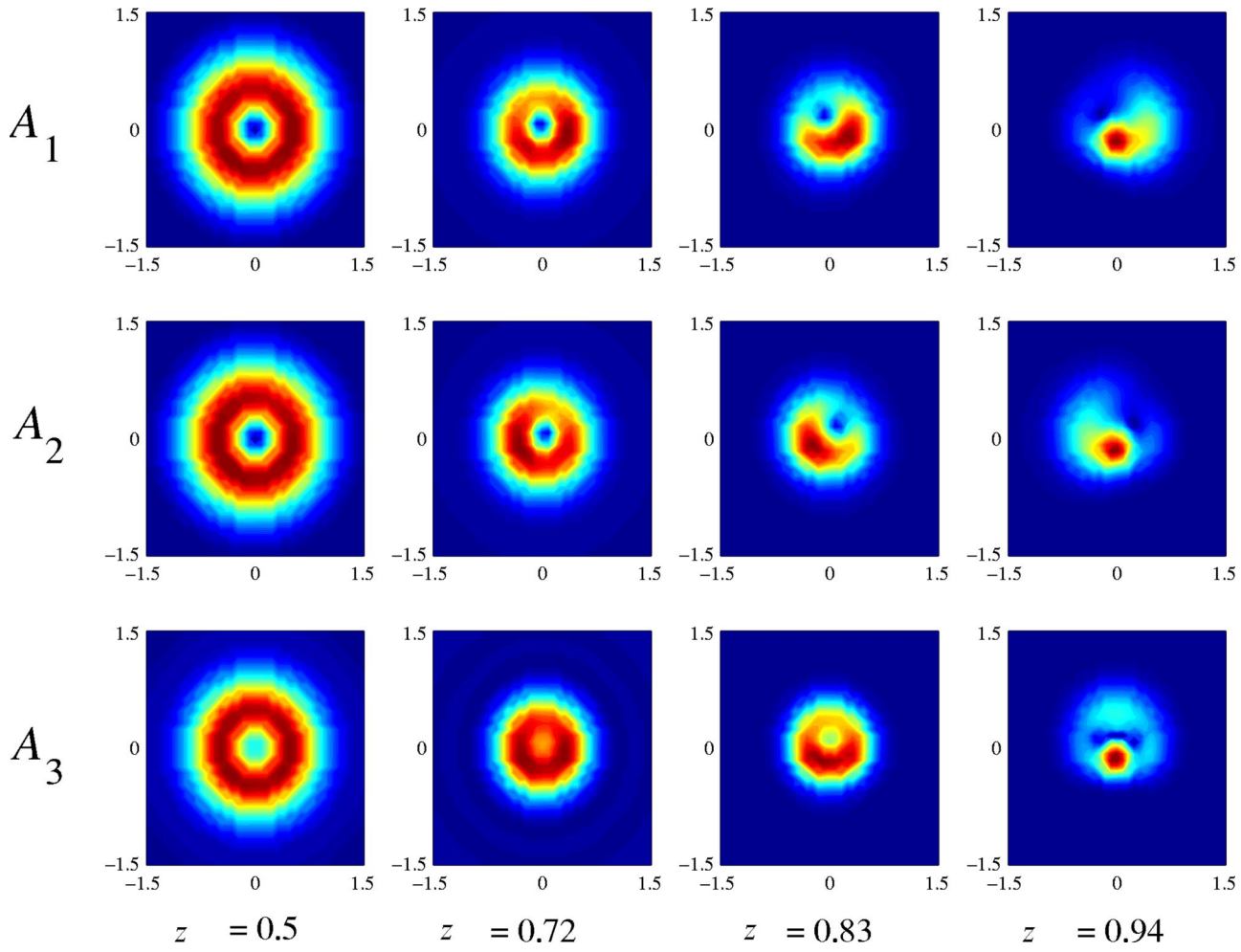

FIG. 2. (Color online) The same as in Fig. 1, but for a negative mismatch, $\alpha=-3$.

bility displayed in Fig. 3 sets in. The radius of this vortex ring is $\rho_0 \simeq 0.19$, which yields $Z_{\mathrm{diffr}} \simeq 0.06$, thus the instability development needs the propagation length $\simeq 16\, Z_{\mathrm{diffr}}$.

After the splitting of the vortex has occurred, the three splinters do not immediately separate; instead, they recombine into a transient pattern of the necklace type. Patterns of this type have recently been found in models with various nonlinearities [28] (in particular, they are especially robust in the case of the same $\chi^{(2)}$: $\chi_{-}^{(3)}$ nonlinearity [29]). In the course of still longer simulations, the necklace observed in Fig. 3 will again split into three segments, but of different sizes, in comparison with the primary ones (not shown here). The recombination and secondary splitting lead to lowering of the pattern's symmetry, from the threefold one in Fig. 3 to a twofold symmetry at a later stage of the evolution.

The comparison to the instability-induced splitting of the vortex soliton suggests a qualitative understanding of the fact that the HV soliton transforms itself into a usual ZV soliton. Indeed, although each FF component may have a trend to split into three segments, the two sets of the splinters (necklaces) would have to rotate in *opposite directions*, which is difficult for them to do. In fact, the opposite angular momenta originally lent to the two FF components can be transferred, because of the direct parametric interaction in the type-II $\chi^{(2)}$ model, into the SH mode, where they mutually cancel.

IV. ANALYSIS OF MODULATIONAL INSTABILITY IN 1D CW STATES WITH "HIDDEN MOMENTUM"

As was mentioned above, the simplest 1D analog of the two-dimensional HV solitons are multicomponent CW solutions with opposite wave numbers, $\pm q$, in two components. However, the analytical investigation of the MI (modulational instability) of such states in the full $\chi^{(2)}$ model of type II turns out to be extremely cumbersome. Much clearer results can be obtained in a simplified model, which corresponds to the cascading limit (the one with large mismatch), i.e., two coupled NLS equations,

$$\left(i\frac{\partial}{\partial z}+\frac{1}{2}\frac{\partial^2}{\partial x^2}\right)A_1+(|A_1|^2+\sigma|A_2|^2)A_1=0, \tag{9}$$

$$\left(i\frac{\partial}{\partial z}+\frac{1}{2}\frac{\partial^2}{\partial x^2}\right)A_2+(|A_2|^2+\sigma|A_1|^2)A_2=0, \tag{10}$$

cf. Eqs. (1) and (2). Here the positive coefficient σ is the *XPM/self-phase modulation (SPM)* ratio, which we keep as a

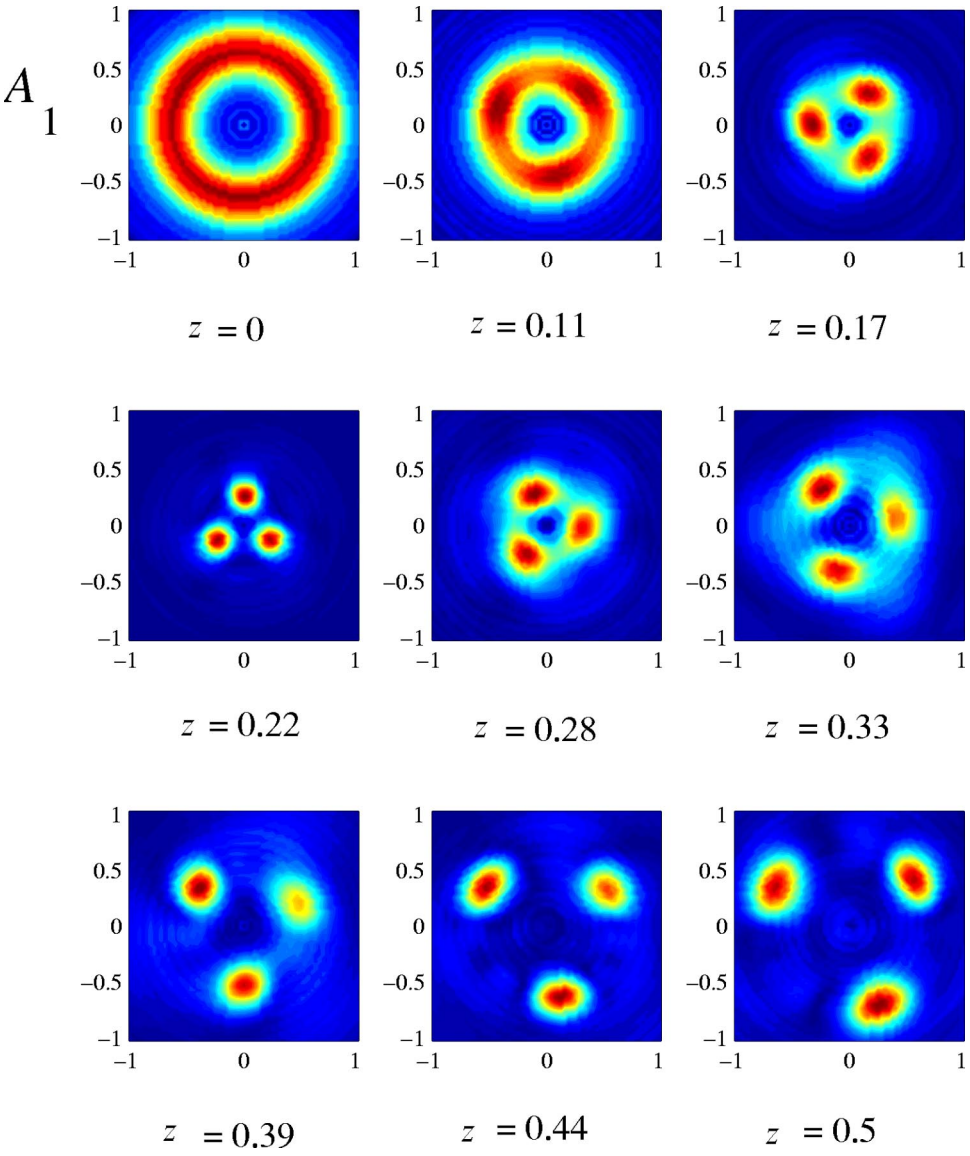

FIG. 3. (Color online) A typical example of the splitting of the ordinary vortex, with $S_{1,2}=1$ and $S_3=2$, in the model without the cubic nonlinearity, into a set of three fragments, that temporarily recombine into a necklace. In this case, $\alpha=-3$ and $\beta=1$. The evolution of only one FF component is shown here, the other fields showing a similar behavior.

free parameter (usual physically relevant values are $\sigma=2/3$ and 2). The solution with "hidden momentum" is

$$A_{1,2}(z,x) = A_0 \exp(ikz \pm iqx), \quad A_0^2 = (k + \tfrac{1}{2}q^2)/(1+\sigma) \tag{11}$$

(the propagation constant k is taken equal in the two components to provide for the symmetric solution). In this connection, it is relevant to mention that two-component solitons of the HV type, with spins $\pm S$ in the two *XPM*-coupled modes, can also be constructed in the 2D version of the system (9) and (10) augmented by self-defocusing quintic terms to provide for the global stability of solitons in the 2D case [32].

For the study of the MI of the solutions (11), we proceed as usual, representing the fields in terms of the amplitude and phase, $A_{1,2} \equiv a_{1,2}(z,x)\exp[i\phi_{1,2}(z,x)]$, and linearizing equations for the perturbations of $a_{1,2}$ and $\phi_{1,2}$. The eigenmodes of the perturbations are subsequently sought for in the form $\sim\exp(\gamma z + ipx)$ with an arbitrary real wave number p. The resulting dispersion relation for the instability growth rate γ is

$$\gamma^2 = \gamma_{\pm}^2(p^2) \equiv p^2\left[A_0^2 - q^2 - \frac{p^2}{4} \pm \sqrt{A_0^2(\sigma^2 A_0^2 - 4q^2) + q^2 p^2}\right], \tag{12}$$

which shows the effect of the hidden momentum q on the MI of the CW solution.

First, the expansion of Eq. (12) for $p^2 \to 0$ demonstrates that the addition of q^2 leads to a *decrease* of the largest instability growth rate for long-wave perturbations,

$$\gamma_+^2 \approx p^2[A_0^2 - q^2 + \sqrt{A_0^2(\sigma^2 A_0^2 - 4q^2)}]. \tag{13}$$

It follows from this expression that the instability at small p^2 is completely eliminated if q^2 belongs to the interval

$$\max\{\sigma - 1, 1\}A_0^2 < q^2 < (\sigma/2)^2 A_0^2, \tag{14}$$

which is actually possible only for $\sigma > 2$. Note also that, in the case of $q^2 > (\sigma A_0/2)^2$, the expressions (12) and (13) yield

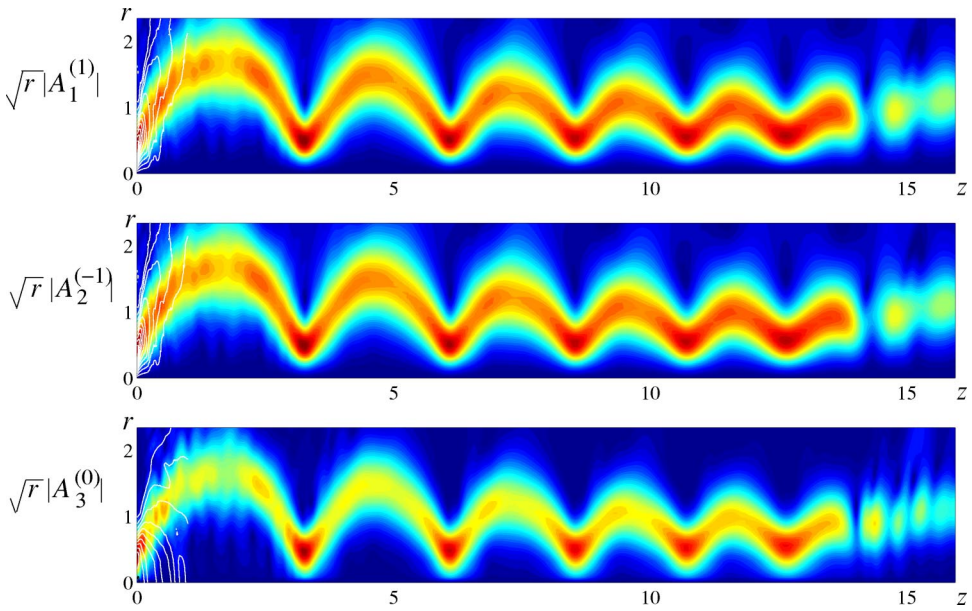

FIG. 4. (Color online) The contour plots display the evolution of the leading azimuthal components $\sqrt{r}A_j^{(S_j)}(r,z)$ $(j=1,2,3)$ of the three amplitudes A_j, which form the hidden-vorticity pulson, with $S_{1,2}=\pm 1$ and $S_3=0$, in the full $\chi^{(2)}:\chi_-^{(3)}$ model (the multiplier $\sqrt{r}$ is added to illustrate the distribution of the integral intensities of the fields, which are $r|A_{1,2,3}|^2$). The vanishing of these components after $\simeq 6$ cycles (at $z\approx 13.5$) corresponds to the destruction of the soliton by the azimuthal instability. In this case, the parameters are $\beta=1$, $\alpha=5$, and $\lambda=0.0045$. The white contours on the left illustrate the diffraction of the input in the absence of nonlinearity.

complex eigenvalues, corresponding to an oscillatory MI, which is not possible when $q=0$.

Another consequence of Eq. (12) is that the value that limits the instability region is

$$p_{\rm cutoff}^2 = 4[q^2 + (1+\sigma)A_0^2] \tag{15}$$

[so that $\gamma^2(p^2)<0$ for $p^2>p_{\rm cutoff}^2$]. Moreover, if $q^2 > (\sigma A_0/2)^2$, there are *two distinct instability intervals*: the one

$$0 < p^2 < A_0^2(4q^2 - \sigma^2 A_0^2)/q^2, \tag{16}$$

in which the instability growth rate is complex, and

$$4[q^2 - (\sigma-1)A_0^2] < p^2 < 4[q^2 + (1+\sigma)A_0^2], \tag{17}$$

wherein it is real. In the region

$$A_0^2(4q^2 - \sigma^2 A_0^2)/q^2 \leqslant p^2 \leqslant 4[q^2 - (\sigma-1)A_0^2], \tag{18}$$

between the intervals (16) and (17), there is no instability.

Finally, the addition of the hidden momentum can also decrease the maximum value $\gamma_{\rm max}$ of the instability growth rate. For instance, in the case of $\sigma=2$ and $q^2=A_0^2$, we find $\gamma_{\rm max}=(\sqrt{3}/2)3A_0\approx 0.866\times 3A_0$ (it is attained at $p=3A_0$), while in the same case, but with $q=0$, a somewhat larger value, $\gamma_{\rm max}=3A_0$, is attained at $p=\sqrt{6}A_0$.

V. STABILIZATION OF VORTICES IN THE FULL MODEL

Many runs of simulations of the full system (1)–(3) with $\lambda>0$ have demonstrated that the HV solitons, as well as the ordinary compound vortices, cannot be completely stabilized under what may be regarded as realistic conditions (in particular, we did not test the stability of the vortices of an extremely large size, where complete stabilization might be expected, as suggested by the results obtained in allied models [2–4,12–14]). However, it is quite possible to find cases when the $\chi_-^{(3)}$ nonlinearity makes both the HV solitons and ordinary vortices practically stable, i.e., the solitons may safely exist over the propagation distance amounting to several dozen of the diffraction lengths, which will render them completely stable objects in any feasible experiment (cf., for instance, experiments in which stable quasi-2D spatiotemporal solitons [30] and optical vortices of the dark-soliton type [31] were found in $\chi^{(2)}$ media—in those cases, the experimentally available propagation distance did not exceed a few diffraction lengths).

As said above, we did not try to start the stability tests by finding numerically exact stationary soliton solutions; instead, the initial configurations were taken in a "reasonable" form, with the aim to keep the simulations closer to the experimental situation in this respect too. As a result, we have observed that, if the initial configuration was limited to a superposition (8) with exactly three components, which correspond either to the HV soliton, with $S_{1,2}=\pm 1$ and $S_3=0$, or the vortex with $S_{1,2}=1$ and $S_3=2$, the "reasonable" input easily self-traps into a pulson which remains stable indefinitely long, if it is not deliberately perturbed.

A. Hidden-vorticity soliton ($S_{1,2}=\pm 1, S_3=0$)

The explicit addition of perturbations in the form of a random mixture of extra angular harmonics gives rise to a slowly developing instability of the solitons. As well as in the previous section, we will first consider the HV soliton. Before being destroyed by the azimuthal instability triggered by added perturbations, it keeps to pulsate at a fixed frequency, as shown in Fig. 4. A cardinal difference from the model without the $\chi_-^{(3)}$ terms (see above) is that now the soliton is robust enough to perform six or seven slow pulsations, whereas in the previous model, it would be destroyed before completing even two cycles of the intrinsic vibrations.

Recall that, in the model with $\lambda=0$, the azimuthal instability transformed the HV soliton into a single ZV soliton (see Fig. 1). In the present case, the outcome of the development of the slow instability is different; as shown in Fig. 5, the HV soliton eventually splits into a set of two ZV ones. A

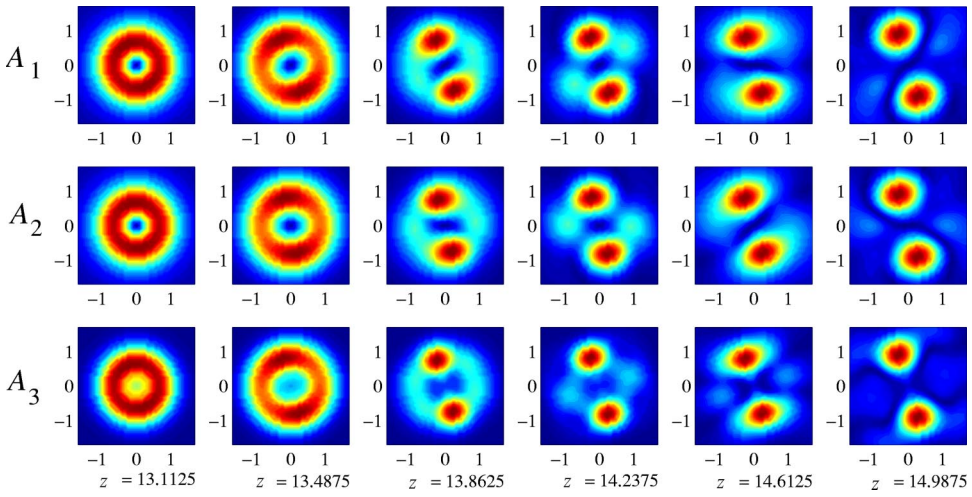

FIG. 5. (Color online) The splitting of the hidden-vorticity soliton into a set of two zero-vorticity solitons caused by the weak azimuthal instability in the same case as in Fig. 4. The three rows of the contour plots show the evolution of intensities of the soliton's fields A_1, A_2, and A_3 at the critical stage of the splitting. At $z < 13$, the initial soliton remains completely stable (featuring long-period persistent radial pulsations).

noteworthy conclusion that follows from Fig. 4 is that the HV soliton, in the form of the ring with the radius $\simeq 0.5$, which corresponds to $Z_{\mathrm{diffr}} \simeq 0.43$ (about twice the values obtained in the case of $\lambda = 0$, cf. Figs. 1 and 2), survives over a propagation distance of about 30 Z_{diffr}, whereas without the $\chi_{-}^{(3)}$ terms, the soliton was destroyed after passing the distance $z \lesssim 15\ Z_{\mathrm{diffr}}$. Note that the radial pulsations of the HV soliton (displayed in Fig. 4) have a very large period, which decreases during the propagation from $\simeq 7.5$ to $\simeq 4.5\ Z_{\mathrm{diffr}}$.

Details concerning the instability-driven growth of the amplitudes of different angular harmonics in the perturbation around the SH component (A_3) of the HV soliton are collected in Fig. 6. The first feature, obvious in the figure, is that the dominant instability is accounted for by a conjugate pair of the harmonics with $p = \pm 2$. With regard to the fact that the SH component of the unperturbed HV soliton has zero vorticity, this precisely complies with the observation that the HV soliton is eventually split by the instability into two ZV solitons (as seen in Fig. 5). Note that, in other models, too, the number of the splinters usually coincides with the azimuthal index of the most unstable perturbation [2,3,12,14,17]. The perturbations with $p = \pm 1$ and $p = \pm 3$ are also formally growing, but they remain insignificant, as their amplitudes stay four orders of magnitude smaller than those of the dominant mode with $p = \pm 2$. It appears that, at a late stage of the instability development, when the linearization is no longer valid, the perturbations with $p = \pm 3$ and $p = \pm 1$ are nonlinearly suppressed by the dominant mode.

Higher-order perturbation harmonics may also play a significant role. In particular, Fig. 6 shows that the modes with $p = \pm 4$ are unstable in the linear approximation (as their growth starts at an early stage), although their linear-growth rate is obviously smaller than that of the main mode, with $p = \pm 2$. However, on the contrary to the above-mentioned perturbations with $p = \pm 1$ and $p = \pm 3$, whose growth is nonlinearly inhibited by the dominant mode, the growth of the harmonics with $p = \pm 4$ is nonlinearly *enhanced*, starting from $z \approx 11$. This observation can be understood, as the $\chi^{(2)}$ nonlinearity directly generates $p = \pm 4$ harmonics from the main $p = \pm 2$ ones.

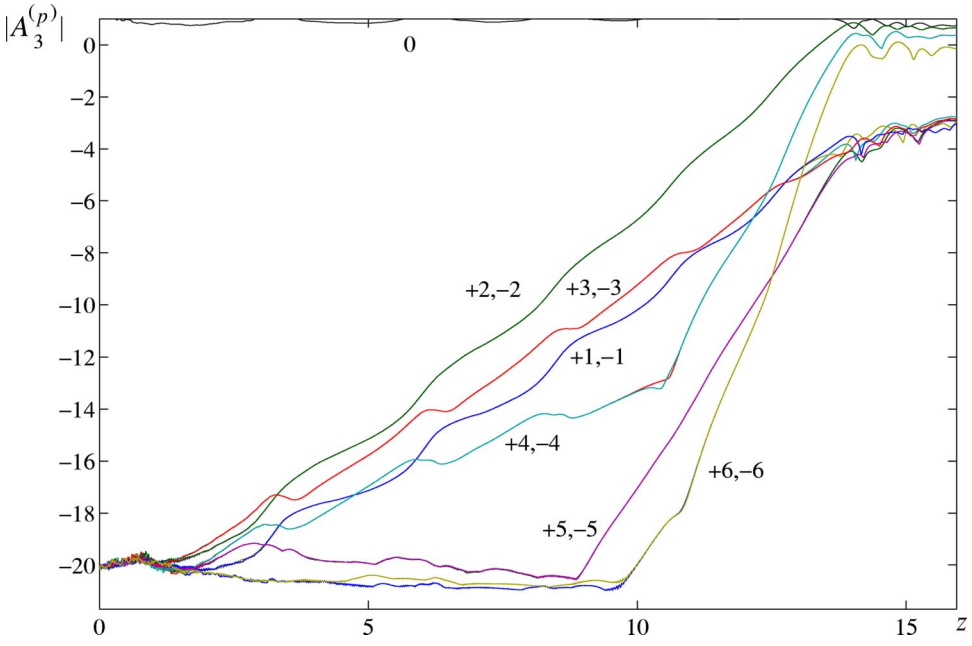

FIG. 6. (Color online) The growth of the amplitudes $|A_3^{(p)}|$ of the angular perturbations in the second-harmonic field [defined as in Eq. (8)] with z is shown on the logarithmic scale, for the same case as in Figs. 4 and 5. The values of the azimuthal index p are indicated near the curves.

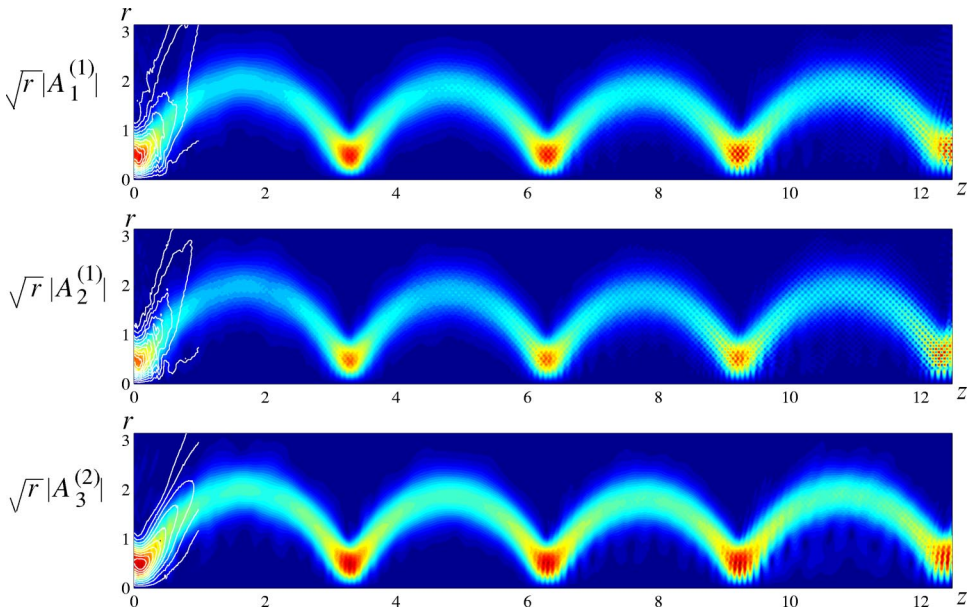

FIG. 7. (Color online) The contour plots display the evolution of the leading azimuthal components $\sqrt{r}A_j^{(S_j)}(r,z)$ $(j=1,2,3)$ of the three amplitudes A_j, which form the vortex pulson, with $S_{1,2}=1$ and $S_3=2$, in the full $\chi^{(2)}:\chi_-^{(3)}$ model (the multiplier $\sqrt{r}$ is added to illustrate the distribution of the integral intensities of the fields, which are $2\pi r|A_{1,2,3}|^2$). The soliton is expected to be destroyed by the azimuthal instability in the course of the further propagation, at about $z=22$. In this case, the parameters are $\beta=1$, $\alpha=-3$, and $\lambda=0.0054$. The white contours on the left illustrate the diffraction of the input in the absence of nonlinearity.

Finally, the modes with $p=\pm5$ and ±6 are linearly stable, as they do not grow up to $z\approx9$, when they suddenly get a boost. It is an obviously nonlinear effect; in particular, the $p=\pm6$ harmonics are directly generated by the $\chi^{(3)}$ terms from the main perturbation mode with $p=\pm2$.

B. Ordinary compound vortex ($S_{1,2}=1, S_3=2$)

Results obtained in related models, with the CQ [2,3,4,17] and type-I $\chi^{(2)}:\chi_-^{(3)}$ [12,14] nonlinearities, suggest that the ordinary vortices, such as the one with $S_3=2S_{1,2}=2$, may be completely stabilized, provided that the size of the vortex soliton is very large. In this work, we did not aim to find completely stable stationary vortices in this way, as the corresponding huge values of the power and diffraction length would be physically unrealistic.

A simpler approach is (as it was done above for the HV solitons) to look for a possibility for self-trapping of practically stable pulsons from a generic input. For instance, choosing $\lambda=0.0054$ and $\beta=1$, $\alpha=-3$, we observed that the vortex remained apparently stable over many diffraction lengths, featuring persistent pulsations in the radial direction, as shown in Fig. 7. In this case, the radius of the vortex ring is $\rho_0\simeq0.5$, which yields $Z_{\rm diffr}\simeq0.43$ and the quasistable propagation is observed up to $z=12.5\approx30\ Z_{\rm diffr}$. An extrapolation of the growth of the perturbations predicts that the splitting of the ring should occur as $z\simeq22\approx50\ Z_{\rm diffr}$.

In fact, the ordinary vortex appears to be even more stable than the HV soliton. Accurate analysis of the numerical data makes it possible to compute the growth rates σ for the amplitudes of different angular harmonics in the perturbation, assuming that the pth one grows as $\exp(\sigma z+ip\theta)$. The result is presented in Fig. 8. As is seen, the most unstable pertur-

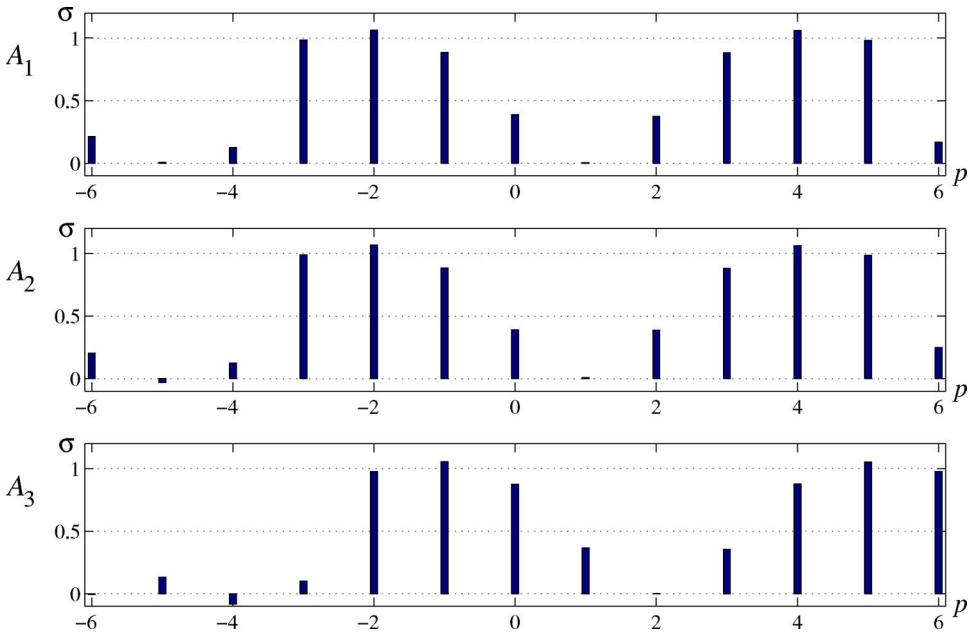

FIG. 8. (Color online) The instability growth rates for different angular harmonics, $\sim\exp(\sigma z+ip\theta)$, in the three components, $A_{1,2}$ and A_3, of the perturbation around the quasistable vortex with $S_{1,2}=1$, $S_3=2$. The parameters are $\lambda=0.0054$, $\beta=1$, and $\alpha=-3$.

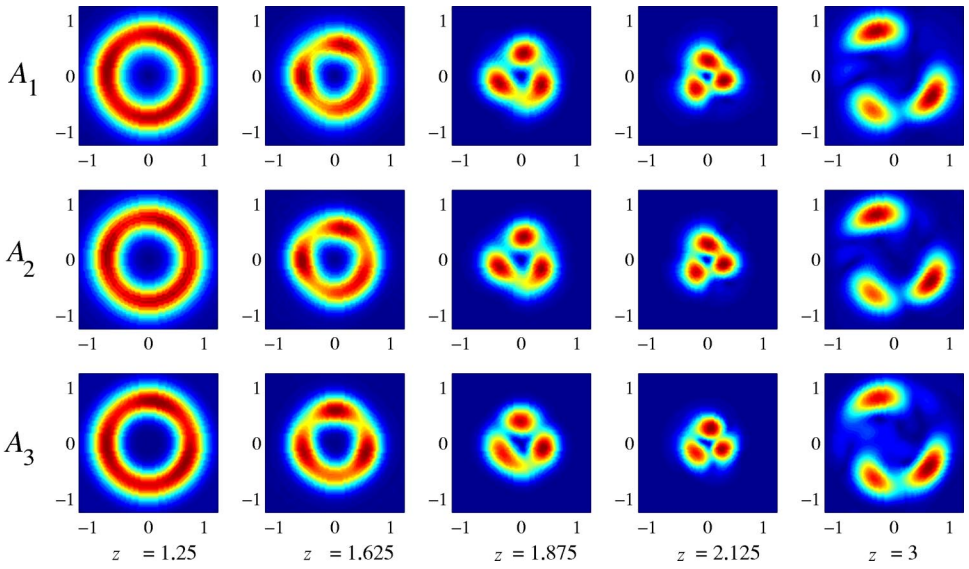

FIG. 9. (Color online) The instability of the ordinary vortex ($S_{1,2}=1, S_3=2$) in the case of $\lambda=0.005$ and $\beta=1$, $\alpha=-3$.

bation modes correspond to $p_{\mathrm{FF}}=(4,-2)$ and $p_{\mathrm{SH}}=(5,-1)$ in the FF and SH fields, respectively. Subtracting the vorticities $S_{1,2}=1$ and $S_3=2$ of the unperturbed FF and SH components from p_{FF} and p_{SH}, respectively, we conclude that relative azimuthal indices of the intrinsic perturbation are ±3, suggesting that the vortex will eventually split into three zero-vorticity solitons, as it has been observed for other values of the parameters (see Fig. 9).

The vortex can also split into a set of four ZV solitons, as shown in Fig. 10. Note that, as well as in Figs. 1–3, initial configurations at $z=0$ in Figs. 9 and 10 have been chosen close to the final stage of the instability development, i.e., they contain large perturbations. Starting with initial configurations that contain small perturbations, we observed that the instability always developed slower than in the model without the cubic terms. In this case, the distance at which the splitting occurs is found to be between 15 and 50 diffraction lengths.

VI. CONCLUSION

In this work, we have considered basic types of 2D vortex solitons in the three-wave model combining the self-defocusing cubic interaction and quadratic interaction of type II. The latter involves two fundamental-frequency (FF) waves and a single second-harmonic (SH) wave. The system can be implemented in a birefringent $\chi^{(2)}$ material on the basis of the quasi-phase-matching technique. The three-wave structure of the model makes it possible to construct a specific type of 2D solitons, namely, the ones with *hidden vorticity* (HV), which carry vorticities ±1 in the FF components, and zero in the SH. In parallel, we have also studied the usual compound vortex with the vorticities $S_3=2S_{1,2}=2$ in the three fields.

In the absence of the self-defocusing cubic nonlinearity, all the vortices are subject to the azimuthal instability within the propagation distance $\lesssim 15\, Z_{\mathrm{diffr}}$ (to accurately define the

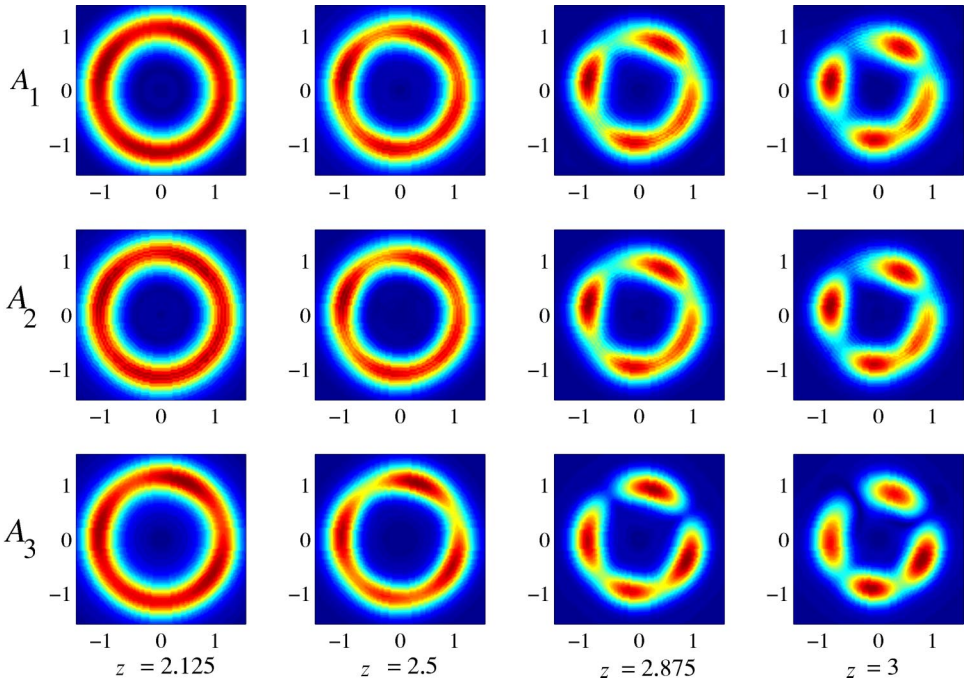

FIG. 10. (Color online) The same as in Fig. 9, but with $\lambda=0.0057$. In this case, the vortex splits into four fragments.

diffraction length Z_{diffr}, we have found an exact solution to the 2D linear Schrödinger equation that describes a spreading localized vortex, which has the meaning of the 2D coherent state with angular momentum in quantum mechanics). This instability transforms the HV soliton into a usual stable 2D zero-vorticity (ZV) pulse (alias, the ground-state soliton), while the ordinary vortex splits into three ZV solitons (they form a transient necklace pattern, which features its own intrinsic dynamics). To better understand this case, we have also developed analytical consideration of its 1D counterpart, viz., the modulational instability of a CW state with the *hidden momentum*, in the form of opposite wave numbers in two coupled components.

In the full model, which includes the cubic terms, both the HV solitons and ordinary compound vortices may be strongly stabilized, persisting over the propagation distance (which can be as large as 30 or even 50 diffraction lengths). Therefore, they are completely stable physical objects, in terms of possible experiments. After very long propagation, the HV soliton splits into two ZV solitons, while the vortex with $S_3=2S_{1,2}=2$ splits into three or four ZV solitons.

The most essential prediction for the experiment, following from the present results, is that observation of an effectively stable 2D soliton with the hidden vorticity is quite possible, in principle, even without the addition of the stabilizing cubic nonlinearity. In the experiment, the radius of the vortex-carrying beam and the FF wavelength are expected to be, respectively, $r\sim 20$ μm and $\lambda_{\mathrm{FF}}\sim 1$ μm, with the respective diffraction length being, in physical units, $Z_{\mathrm{diffr}}\sim(2\pi/\lambda)\sqrt{3}r^2\simeq 0.5$ cm; hence, a sample admitting the propagation length up to $z\sim 20$ cm will be necessary.

ACKNOWLEDGMENT

The work of one of the authors (B.A.M.) was supported, in part, by Grant No. 8006/03 from the Israel Science Foundation.

[1] M. Quiroga-Teixeiro and H. Michinel, J. Opt. Soc. Am. B **14**, 2004 (1997).
[2] I. Towers, A. V. Buryak, R. A. Sammut, B. A. Malomed, L.-C. Crasovan, and D. Mihalache, Phys. Lett. A **288**, 292 (2001); B. A. Malomed, L.-C. Crasovan, and D. Mihalache, Physica D **161**, 187 (2002).
[3] L.-C. Crasovan, B. A. Malomed, and D. Mihalache, Pramana, J. Phys. **57**, 1041 (2001).
[4] R. L. Pego and H. A. Warchall, J. Nonlinear Sci. **12**, 347 (2002).
[5] T. A. Davydova and A. I. Yakimenko, J. Opt. A, Pure Appl. Opt. **6**, S197 (2004).
[6] F. Smektala, C. Quemard, V. Couderc, and A. Barthélémy, J. Non-Cryst. Solids **274**, 232 (2000); K. Ogusu, J. Yamasaki, S. Maeda, M. Kitao, and M. Minakata, Opt. Lett. **29**, 265 (2004).
[7] C. Zhan, D. Zhang, D. Zhu, D. Wang, Y. Li, D. Li, Z. Lu, L. Zhao, and Y. Nie, J. Opt. Soc. Am. B **19**, 369 (2002).
[8] G. Boudebs, S. Cherukulappurath, H. Leblond, J. Troles, F. Smektala, and F. Sanchez, Opt. Commun. **219**, 427 (2003); F. Sanchez, G. Boudebs, S. Cherukulappurath, H. Leblond, J. Troles, and F. Smektala, J. Nonlinear Opt. Phys. Mater. **13**, 7 (2004).
[9] Y.-F. Chen, K. Beckwitt, F. W. Wise, and B. A. Malomed, Phys. Rev. E **70**, 046610 (2004).
[10] W. J. Firth and D. V. Skryabin, Phys. Rev. Lett. **79**, 2450 (1997); L. Torner and D. V. Petrov, Electron. Lett. **33**, 608 (1997).
[11] D. V. Petrov, L. Torner, J. Martorell, R. Vilaseca, J. P. Torres, and C. Cojocaru, Opt. Lett. **23**, 1787 (1998).
[12] I. Towers, A. V. Buryak, R. A. Sammut, and B. A. Malomed, Phys. Rev. E **63**, 055601(R) (2001).
[13] B. A. Malomed, G. D. Peng, P. L. Chu, I. Towers, A. V. Buryak, and R. A. Sammut, Pramana, J. Phys. **57**, 1061 (2001).
[14] D. Mihalache, D. Mazilu, B. A. Malomed, and F. Lederer, Phys. Rev. E **69**, 066614 (2004).
[15] G. I. Stegeman, D. J. Hagan, and L. Torner, Opt. Quantum Electron. **28**, 1691 (1996).
[16] C. Etrich, F. Lederer, B. A. Malomed, T. Peschel, and U. Peschel, Prog. Opt. **41**, 483 (2000); A. V. Buryak, P. Di Trapani, D. V. Skryabin, and S. Trillo, Phys. Rep. **370**, 63 (2002).
[17] D. Mihalache, D. Mazilu, I. Towers, B. A. Malomed, and F. Lederer, J. Opt. A, Pure Appl. Opt. **4**, 615 (2002); D. Mihalache, D. Mazilu, B. A. Malomed, and F. Lederer, J. Opt. B: Quantum Semiclassical Opt. **6**, S341 (2004).
[18] Z. H. Musslimani, M. Segev, D. N. Christodoulides, and M. Soljacic, Phys. Rev. Lett. **84**, 1164 (2000); C. Weilnau, W. Krolikowski, E. A. Ostrovskaya, M. Ahles, M. Geiseer, G. McCarthy, C. Denz, Yu. S. Kivshar, and B. Luther-Davies, Appl. Phys. B: Lasers Opt. **72** 723 (2001); A. S. Desyatnikov, D. Neshev, Y. S. Kivshar, G. McCarthy, W. Krolikowski and B. Luther-Davies, J. Opt. Soc. Am. B **19**, 586 (2002).
[19] M. Chen, D. J. Kaup, and B. A. Malomed, Phys. Rev. E **69**, 056605 (2004).
[20] K. J. Blow, N. J. Doran, and D. Wood, Opt. Lett. **12**, 202 (1987).
[21] C. B. Clausen, O. Bang, and Y. S. Kivshar, Phys. Rev. Lett. **78**, 4749 (1997); J. F. Corney and O. Bang, Phys. Rev. E **64**, 047601 (2001); O. Bang, C. B. Clausen, P. L. Christiansen, and L. Torner, Opt. Lett. **24**, 1413 (1999); S. K. Johansen, S. Carrasco, L. Torner, and O. Bang, Opt. Commun. **203**, 393 (2002).
[22] N. C. Panoiu, D. Mihalache, D. Mazilu, F. Lederer, and R. M. Osgood, Phys. Rev. E **68**, 016608 (2003); N. C. Panoiu, D. Mihalache, H. Rao, and R. M. Osgood, *ibid.* **68**, 065603(R) (2003); N. C. Panoiu, D. Mihalache, D. Mazilu, F. Lederer, R. M. Osgood, J. Opt. B: Quantum Semiclassical Opt. **6**, S351 (2004).
[23] H. Leblond, J. Phys. A **31**, 3041 (1998); H. Leblond, *ibid.* **31**, 5129 (1998).
[24] V. V. Steblina, A. V. Buryak, R. A. Sammut, D. Y. Zhou, M. Segev, and P. Prucnal, J. Opt. Soc. Am. B **17**, 2026 (2000); J.

P. Torres, S. L. Palacios, L. Torner, L. C. Crasovan, D. Mihalache, and I. Biaggio, Opt. Lett. **27**, 1631 (2002).

[25] K. Beckwitt, Y.-F. Chen, F. W. Wise, and B. A. Malomed, Phys. Rev. E **68**, 057601 (2003).

[26] I. N. Towers, B. A. Malomed, and F. W. Wise, Phys. Rev. Lett. **90**, 123902 (2003).

[27] D. Mihalache, D. Mazilu, L.-C. Crasovan, I. Towers, B. A. Malomed, A. V. Buryak, L. Torner, and F. Lederer, Phys. Rev. E **66**, 016613 (2002).

[28] M. Soljacic, S. Sears, and M. Segev, Phys. Rev. Lett. **81**, 4851 (1998); M. Soljacic and M. Segev, Phys. Rev. E **62**, 2810 (2000); **86**, 420 (2001); A. S. Desyatnikov and Yu. S. Kivshar, *ibid.* **88**, 053901 (2002); Y. V. Kartashov, G. Molina-Terriza, and L. Torner, J. Opt. Soc. Am. B **19**, 2682 (2002); D. Mihalache, D. Mazilu, L.-C. Crasovan, B. A. Malomed, F. Lederer, and L. Torner, Phys. Rev. E **68**, 046612 (2003); D. Mihalache, D. Mazilu, L.-C. Crasovan, B. A. Malomed, F. Lederer, and L. Torner, J. Opt. B: Quantum Semiclassical Opt. **6**, S333 (2004).

[29] Y. V. Kartashov, L.-C. Crasovan, D. Mihalache, and L. Torner, Phys. Rev. Lett. **89**, 273902 (2002); L.-C. Crasovan, Y. V. Kartashov, D. Mihalache, L. Torner, Yu. S. Kivshar, and V. M. Perez-García, Phys. Rev. E **67**, 046610 (2003).

[30] X. Liu, L. J. Qian, and F. W. Wise, Phys. Rev. Lett. **82**, 4631 (1999); X. Liu, K. Beckwitt, and F. Wise, Phys. Rev. E **62**, 1328 (2000).

[31] P. Di Trapani, W. Chinaglia, S. Minardi, A. Piskarskas, and G. Valiulis, Phys. Rev. Lett. **84**, 3843 (2000).

[32] A. S. Desyatnikov, D. Mihalache, D. Mazilu, B. A. Malomed, C. Denz, and F. Lederer, Phys. Rev. E **71**, 026615 (2005).